

# Experimental Investigation on the Influence of Tool Geometry in Minimum Chip Thickness of Microendmilling Using Cutting Force Analysis



M. Prakash, M. Kanthababu, A. Arul Jeya Kumar,  
and V. Prasanna Venkadesan

**Abstract** Minimum uncut ( $t_m$ ) chip thickness is the promising factor of the microendmilling process, which is affected by many factors. The tool geometry is one among them. In this work, the effect of different tool geometries, two flutes and four flutes of microendmill (500  $\mu\text{m}$  diameter), are investigated, during slot milling of copper alloy (BSS 249) by considering the surface roughness ( $R_a$ ) and cutting forces. The results show that the feed rate has more impact on the  $R_a$ . A higher order of  $R_a$  value is observed with the two flutes microendmill than that of with four flutes microendmill, due to the closer tool path generation of the subsequent passes of the four flutes. It is also observed that the transition of chip formation from interrupted chips to continuous chips has occurred with two flutes and four flutes. From the cutting forces analysis, it is found that the feed force ( $F_y$ ) is greater than that of the transverse forces ( $F_x$ ) irrespective of the tool geometry. The behaviour of cutting forces also helps to identify the minimum uncut chip thickness ( $t_m$ ). The angular shifting of the cutting forces is also observed concerning the tool geometry. The material removal mechanism reveals that the ploughing effect is more dominant than that of the shearing effect with two flutes microendmill. The present investigations have shown that four flutes microendmill is more suitable for tool-based microendmilling in order to achieve better  $R_a$  with minimum cutting forces.

**Keywords** Microendmill · Tool geometry · Surface roughness · Cutting forces · Uncut chip thickness

---

M. Prakash (✉) · A. Arul Jeya Kumar  
SRM Institute of Science and Technology, Kattankulathur, India  
e-mail: [prakashmuniyandi@gmail.com](mailto:prakashmuniyandi@gmail.com)

M. Kanthababu  
CEG, Anna University, Chennai, India

V. Prasanna Venkadesan  
Indian Institute of Information Technology Design & Manufacturing, Kancheepuram, India

## 1 Introduction

Recently, with more demand for accurate and precise micro-components, the importance of tool-based micromachining processes has been increased in the number of fields, such as medical, aerospace and automobile [1]. Among the tool-based micromachining processes, microendmilling is used for manufacturing the micro-components like microsurgical equipment, micro-impellor and micro-nozzle. Microendmilling uses microendmills with diameter in the sub-millimetre range. The edge radius of a typical microendmill is in the order of a few microns, and also, the uncut chip thickness ( $t$ ) is usually lesser than the edge radius. Due to the size of the microendmill, it is very difficult to achieve the quality in the finished components. Previous investigations have indicated that the tool life in the tool-based micromachining is unpredictable, and also it fails prematurely [2–4].

Microendmilling distinguished from macro-regime machining in terms of size effect and  $t$  [5]. The  $t$  is greatly influenced by the chip formation process in the microendmilling. If the  $t$  is less than the minimum uncut chip thickness ( $t_m$ ) (i.e. 0.33 of nose radius ( $r_e$ )), ploughing is found to be dominating than that of the shearing [4], which resulted in the increase of cutting forces. New by et al. [5] made an attempt to calculate the uncut chip thickness ( $t$ ) based on the feed per flute and cutting edge radius, which is shown in Eqs. 1 and 2.

$$\text{Uncut chip thickness } (t) = t_x \sin \alpha - \frac{n}{2\pi r_e} t_x^2 \sin \alpha \cos \alpha + \frac{1}{2r_e} t_x^2 \cos^2 \alpha \quad (1)$$

where

$$t_x = \frac{F \times 1000}{S \times n} \quad (2)$$

where  $t$ —uncut chip thickness ( $\mu\text{m}$ ),  $t_x$ —feed per flute ( $\mu\text{m}$ ),  $F$ —feed rate (mm/min),  $S$ —rotational speed (rpm),  $n$ —number of flute,  $\alpha$ —tool rotational angle,  $r_e$ —tool nose radius.

Generally, in tool-based micromachining processes the quality of the machined surface is mostly affected by the characteristics of cutting forces, which are mostly affected by the tool geometry [6]. Therefore, there is a need for more investigation on the effect of cutting forces generated during microendmilling. However, few attempts were made by researchers to study the effect of cutting forces in conventional/macro-regime endmilling [6–11].

Literature review related to the studies on the effect of tool geometry on the cutting forces is briefly presented here. Fang et al. [6] carried out the experimental investigations to study the effect of different tool geometries such as two flutes, triangle type and semicircular type and its failure modes using cutting force signals in the microendmilling of brass material. They have observed that the tool rigidity is much higher with the triangular-based microendmill, than that of the two flutes

microendmill. However, the machining quality is found to be poor with triangular-based microendmill than that of two flutes types of microendmill. Filiz et al. [7] investigated the effect of two flutes of the microendmill with cutting forces during microendmilling of copper. They have found that the  $t_m$  and associated ploughing effects induce variations in the cutting forces. Li et al. [8] carried out experimental analysis on the tool wear and surface roughness using two flutes 0.1 mm diameter microendmill in microendmilling of OFHC Copper. They have observed that, the effect of the  $t_m$  on the surface roughness is found to be lower, when the feed per tooth is lower than that of the  $t_m$ . Lai et al. [9] developed an analytical model based on the finite element simulations for microendmilling. It is resulted that the edge radius is the major factor for the  $t_m$ . Bissacco et al. [10] found that during microendmilling the effect of machining process parameters is not similar to that of macro-regime milling due to the size effect and the reduced stiffness of the microendmill. These differences are mainly due to the changes in physical phenomena,  $t_m$  and microstructure of the work material.

From the literature, it is observed that during microendmilling, the tool geometry plays a significant role in terms of generation of the  $t_m$  subsequently cutting forces and surface roughness. It is also necessary to understand the microendmilling mechanism with respect to the tool geometry [11–14]. From the literature review, it is also observed that the effect of cutting forces in microendmilling is not yet fully explored. In addition to the cutting forces, the other factors that are affected by the tool geometry in microendmilling are entry and exit of the flutes, which occurs repeatedly during the cutting process, run out of the tool tip,  $t_m$ , ploughing, indentation, elastic recovery, etc. [15–30].

Therefore, in this work investigations are carried out to identify the effect of different tool geometries such as two flutes and four flutes of the microendmill by analysing the behaviour of uncut chip thickness ( $t$ ) along with the cutting forces (transverse force ( $F_x$ ) and feed force ( $F_y$ )).

## 2 Experimental Set-up

Microendmilling was performed using MIKROTOOLS made multi-process machine tool driven by a 100 W AC servo drive motor that can provide a rotational speed up to 5000 rpm. The X-Y table has optical linear scale with resolution of 0.1  $\mu\text{m}$ . Two flutes carbide microendmill (Model: E9661; Make: AXIS, India) and four flutes carbide microendmill (Model: E9671; Make: AXIS, India) of 500  $\mu\text{m}$  diameter each coated with aluminium titanium nitride (AlTiN) of 400 nm thickness are used for the experimentation (Fig. 2). The workpiece material used in the work is copper alloy (BSS 249), and its chemical composition is copper 55.70%, lead 3.30% and zinc 38.58%. Vickers's hardness of the workpiece is 146.10 HV. The workpiece is mounted on the worktable of the machine, and the microendmill is clamped to the spindle unit of the machine (Fig. 1).

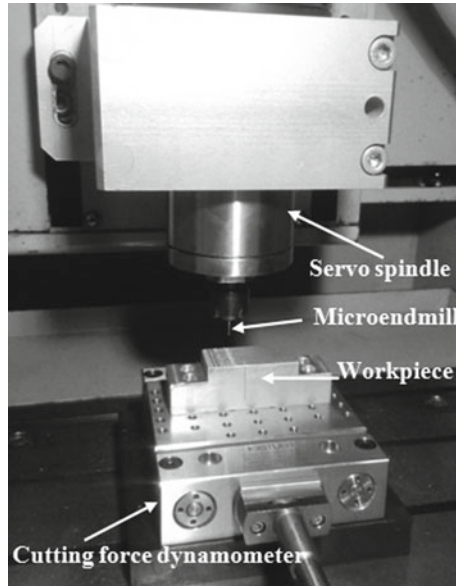


**Fig. 1** Experimental set-up closer view

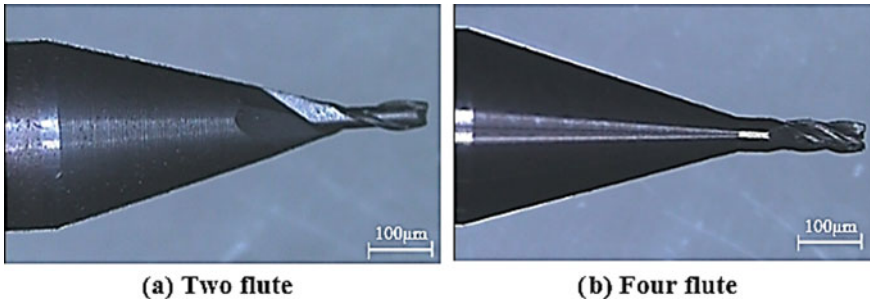


**Fig. 2** Photograph of the microendmills

Experiments are conducted as per the design of experiments approach (DoE), using the  $L_{16}$  orthogonal array, and optimal parameters based on the surface roughness such as rotational speed of 2800 rpm, feed rate of 10 mm/min and depth of cut (DOC) of  $50\ \mu\text{m}$  are obtained [27]. The above-optimized cutting parameters are used to analyse the effect of different tool geometry, namely two flutes and four flutes.

The surface roughness ( $R_a$ ) is measured on the machined surfaces at three different locations (entry, middle and exit along the length of cut) in the feed direction using non-contact instrument Talysurf CCI Lite, with  $0.983\ \mu\text{m}$  cut of length and  $333\ \mu\text{m}$  traverse length. The average value is recorded and given in Table 1.

**Table 1** Allocation of input parameters in L<sub>16</sub> OA and experimental results

Ex. No.	Speed [S] (rpm)	Feed [F] (mm/min)	Surface roughness [R <sub>a</sub> ] (μm)		Cutting Forces (N)			
					Two flutes		Four flutes	
			Two flutes	Four flutes	[F <sub>x</sub> ]	[F <sub>y</sub> ]	[F <sub>x</sub> ]	[F <sub>y</sub> ]
1	700	5	0.194	0.145	0.037	0.771	0.400	0.470
2	700	10	0.163	0.126	0.583	0.771	0.819	0.444
3	700	15	0.169	0.159	1.050	0.875	1.500	0.695
4	700	20	0.219	0.204	2.376	2.498	2.910	1.320
5	1400	5	0.192	0.106	0.057	0.955	0.545	0.389
6	1400	10	0.122	0.101	0.117	0.300	0.491	0.529
7	1400	15	0.108	0.093	0.844	0.910	1.140	0.623
8	1400	20	0.174	0.108	0.759	0.774	1.107	0.292
9	2100	5	0.163	0.079	0.121	0.903	0.538	0.011
10	2100	10	0.088	0.071	0.390	0.827	0.809	0.381
11	2100	15	0.104	0.063	0.084	0.449	0.611	0.351
12	2100	20	0.114	0.086	0.229	0.690	0.617	0.354
13	2800	5	0.125	0.062	0.137	0.938	0.336	0.293
14	2800	10	0.091	0.075	0.178	0.675	0.468	0.388
15	2800	15	0.076	0.066	0.134	0.487	0.425	0.375
16	2800	20	0.101	0.067	0.001	0.419	0.382	0.257

The cutting forces in transverse ( $F_x$ ), feed ( $F_y$ ) and axial ( $F_z$ ) direction were measured using piezoelectric cutting force dynamometer (Fig. 1). The dynamometer (Make: Kistler, Model: 9256C2) is mounted on the fixture unit of the machine and then connected to a charge amplifier, which in turn connected to a PC for acquiring the data using data acquisition system with DynoWare software (Fig. 1). The directions of cutting forces ( $F_x$ ,  $F_y$  and  $F_z$ ) are measured using the dynamometer which is shown in Fig. 3.  $F_x$ ,  $F_y$  and  $F_z$  are measured along the X-, Y- and Z-axes, respectively. The cutting force signals are measured at the sampling rate of 1000 Hz with the regular intervals of 120 s. During microendmilling (slot milling), it is observed that both downmilling and upmilling occurs, which is also similarly observed by Kang et al. [20]. The schematic indicates the direction of cutting forces measured during downmilling and upmilling is shown in Fig. 4a, b, respectively. Figure 4 indicates that ploughing occurs during the rotation of the microendmill from A to B and E to D regions during upmilling and downmilling, respectively, whereas shearing occurs during the rotation of the microendmill, from B to C and C to D regions during upmilling and downmilling, respectively.

From the preliminary studies, it is observed that the axial force is found to be non-significant in all the machining conditions due to the lower order of depth of cut (i.e. 50 μm), which is also similarly observed by Bissacco et al. [10]. Therefore, the

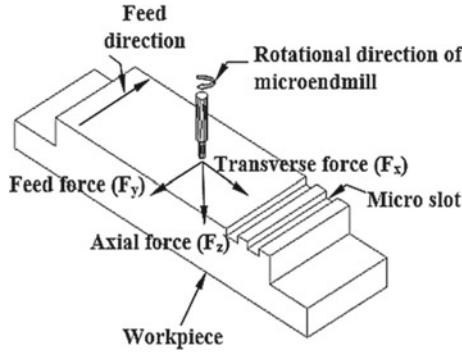
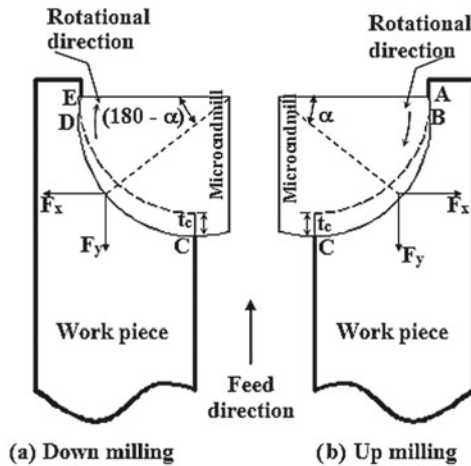


Fig. 3 Schematic diagram of the cutting force components in microendmilling



A to B: Ploughing ( $t < t_m$ ), B to C: Upmilling ( $t \geq t_m$ ),  
 C to D: Downmilling ( $t \geq t_m$ ), E to D: Ploughing ( $t < t_m$ )

$t$  – Uncut chip thickness,  $t_c$  – Maximum uncut chip thickness,  
 $t_m$  – Minimum uncut chip thickness,  $\alpha$  – Tool rotational angle

Fig. 4 Schematic of the direction of cutting forces in the workpiece in microendmilling

axial force is not considered for further analysis. The resultant force is also calculated by considering transverse and feed force using Eq. 3, which is given as

$$\text{Resultant force } (F_r) = \sqrt{F_x^2 + F_y^2} \tag{3}$$

### 3 Results and Discussion

The effect of two different microendmill geometries such as two flutes and four flutes during microendmilling on the surface roughness ( $R_a$ ), the uncut chip thickness ( $t$ ), and cutting forces ( $F_x$  and  $F_y$ ) is analysed. They are briefly presented below.

#### 3.1 Surface Roughness ( $R_a$ )

Experiments are carried out by varying the rotational speed and feed rate with constant depth of cut of 50  $\mu\text{m}$ . The effect of two different tool geometries such as two flutes and four flutes of the microendmill at various cutting parameters on the  $R_a$  is shown in Fig. 5. Typical surface topography of the machined surface with two flutes and four flutes of microendmill is shown in Fig. 6. From Figs. 5 and 6, it is observed that  $R_a$  values are found to be lower in the four flutes microendmill than that of two flutes microendmill. This may be due to the formation of continuous chips with four flutes than that of the two flutes (Fig. 7). This may also be due to the formation of closer tool path (i.e. due to the increase in number of flutes in the four flutes microendmill) for subsequent passing of microendmill in the feed direction as illustrated by Bao et al. [16]. In the case of microendmilling with two flutes, higher  $R_a$  is observed due to interrupted chip formation (Fig. 7). It is also observed that  $R_a$  is found to be decreased with the increase in the rotational speeds up to the feed rate of 12 mm/min both with the two flutes and four flutes microendmill. However,  $R_a$  is found to be increased as the feed rate increases beyond 12 mm/min. There is no significant variation in  $R_a$  at the higher rotational speed above 1400 rpm with increase in feed rate beyond 12 mm/min. Therefore, in order to achieve a better  $R_a$ , four flutes microendmill

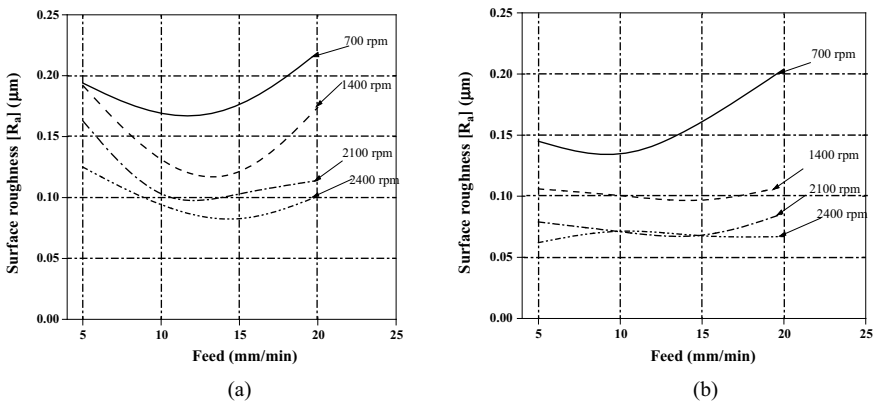


**Fig. 5** Tool geometry effect on surface roughness in microendmilling. **a** Two flutes microendmill. **b** Four flutes microendmill

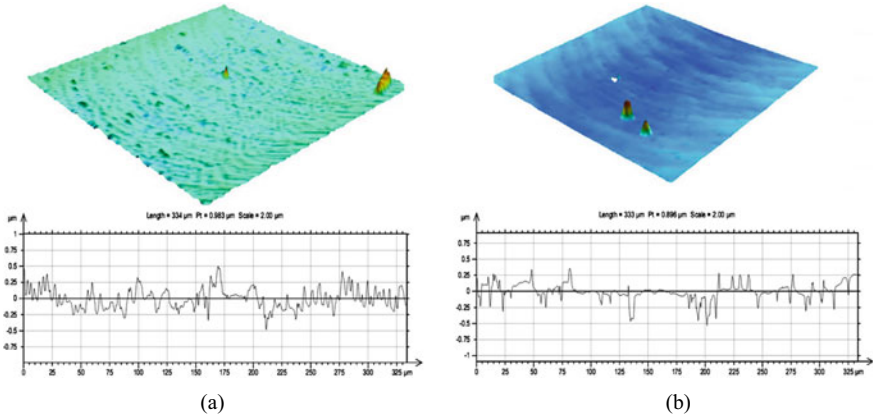


**Fig. 6** Typical surface topography of the machined surface in microendmilling. **a** Two flutes microendmill. **b** Four flutes microendmill

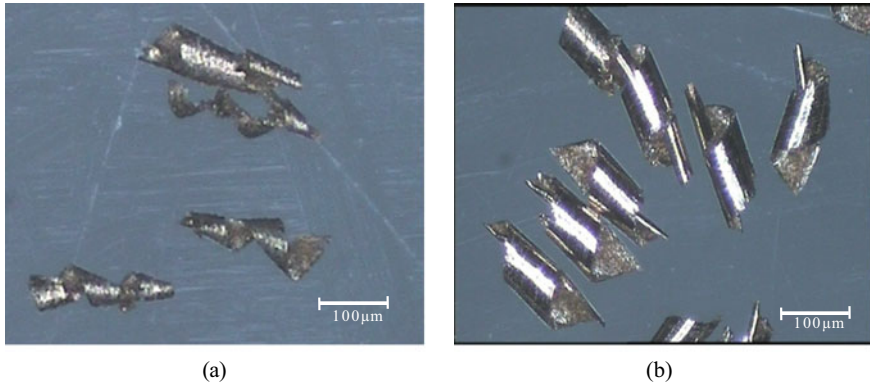


**Fig. 7** Typical chips obtained in microendmilling. **a** Two flutes microendmill. **b** Four flutes microendmill

with higher rotational speed along with moderate feed rate are found to be highly desirable.

### 3.2 Uncut Chip Thickness ( $t$ )

The behaviour of the uncut chip thickness ( $t$ ) is analysed during the half rotation for both two flutes and four flutes microendmill by varying the rotational speed. Figure 8 indicates the two regions of material removal mechanism in microendmill based on the uncut chip thickness ( $t$ ) such as ploughing (regions A to B and D to E)



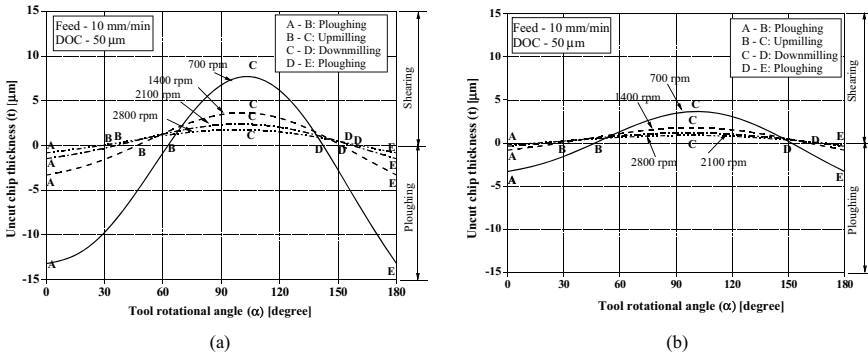


**Fig. 8** Behaviour of uncut chip thickness of different tool geometry with varying speed in microendmilling. **a** Two flutes microendmill. **b** Four flutes microendmill

and shearing (regions B to C and C to D). During shearing (regions B to C and C to D), both upmilling and downmilling occurred.

Figure 8a indicates that in the case of two flutes microendmill, with the increase in the rotational speed and there is a decrease in the thickness value of uncut chip thickness ( $t$ ). However, ploughing (regions A to B and D to E) is found to be more dominant than that of the shearing (regions B to C and C to D). This is also reflected in the formation of interrupted chip (Fig. 6a), in which the chips are not formed until the uncut chip thickness ( $t$ ) reaches the minimum uncut chip thickness ( $t_m$ ) during the subsequent passes of microendmill along the feed direction. This indicates that the chip formation did not occur during the single pass of the microendmill, and therefore, subsequent passes are required for the chip formation process.

Figure 8b indicates the behaviour of uncut chip thickness ( $t$ ) with four flutes microendmill with the increase in the rotational speed. From the Fig. 8b, both ploughing (regions A to B and D to E) and shearing (regions B to C and C to D) are observed during the half tool rotation of the microendmill, irrespective of the rotational speed (Fig. 8b). However, the size of uncut chip thickness ( $t$ ) is found to be lesser than that of the two flutes microendmilling. It is also observed that in the four flutes microendmill, the shearing (regions B to C and C to D) is found to be more dominating than that of the ploughing (regions A to B and D to E), which is also reflected in the formation of continuous chip (Fig. 7b).

Figure 9a, b shows the effect of feed rate with respect to two flutes and four flutes microendmill on the uncut chip thickness ( $t$ ) during the half rotation of the microendmill. Both ploughing (regions A to B and D to E) and shearing (regions B to C and C to D) are observed during the half tool rotation of the microendmill, irrespective of the rotational feed rate (Fig. 9). From Fig. 9a, it is observed that the uncut chip thickness ( $t$ ) is found to increase with the increase in the feed rate. It is also observed that with the increase in the feed rate, ploughing effect dominates the shearing effect. However, in the case of microendmilling with four flutes microendmill (Fig. 9b), it is found that the size of uncut chip thickness ( $t$ ) and the effect of ploughing are

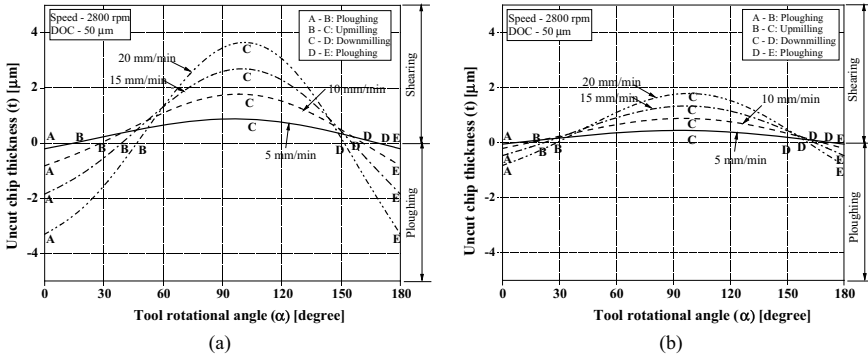


**Fig. 9** Behaviour of uncut chip thickness of different tool geometry with varying feed in microendmilling. **a** Two flutes microendmill. **b** Four flutes microendmill

lesser than that of with the two flutes microendmill. This may be due to the closer trochoidal tool path generation of the four flutes microendmill than that of two flutes microendmill, which is also similarly observed by Newby et al. [5]. These results indicate that the tool path generation in microendmilling significantly depends on the number of flutes and the feed rate, which is also similarly observed by Tansel et al. and Bao et al. [14, 16]. Higher feed rate with more number of flutes results in continuous chip formation, which is also similarly observed in the conventional endmilling [11–13].

### 3.3 Cutting Forces

Figures 10 and 11 show the typical cutting forces in the transverse and feed directions,

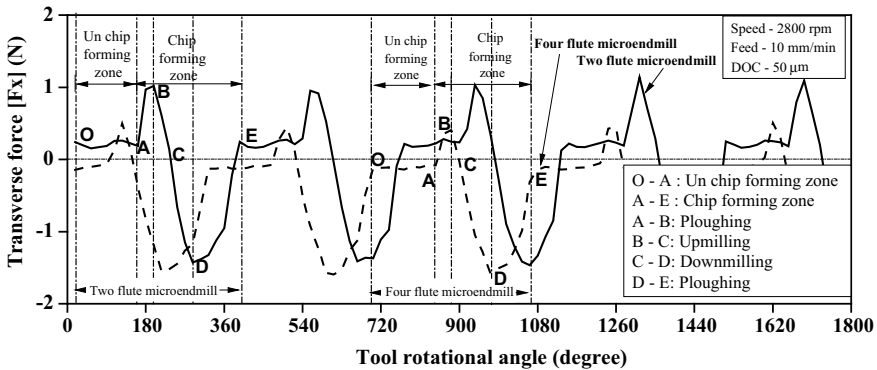


**Fig. 10** Typical transverse force acquired during microendmilling

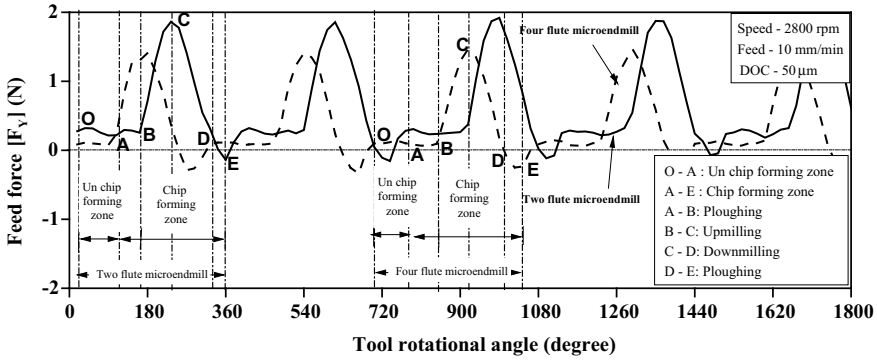


Fig. 11 Typical feed force acquired during microendmilling

respectively, for two flutes and four flutes microendmill. From Figs. 10 and 11, it is observed that the signature of the transverse force and feed force signals for both two flutes and four flutes microendmill is found to be in increasing and decreasing trend both in positive and negative directions with respect to the tool rotational angle. However, from Figs. 10 to 11, it is observed that, at the earlier stages with four flutes microendmill there is the significant angular shift in cutting forces at the region of unchip forming zone (O to A), where no chips are formed, than that of with the two flutes microendmill. This may be due to the closer trochoidal tool path of the four flutes microendmill than that of two flutes microendmill. This is well agreed with the result of Bao et al. [16]. It is also observed from Figs. 10 and 11, that the signature of the cutting force signal during unchip forming zone (O to A) and chip forming zone (A to E) is found to be different from the four flutes microendmill than that of two flutes microendmill, due to the change in frequency of contact of two flutes microendmill than that of four flutes microendmill.

From Fig. 10, it is observed that the direction changes in the transverse force from upmilling (B to C) to downmilling (C to D) with both two flutes and four flutes microendmill as shown in Fig. 4. However, the magnitude of the transverse force during the upmilling is lower in the case of four flutes microendmill. But in the case of downmilling, there is no significant variation is observed. Transverse force due to ploughing (regions A to B and D to E) is more dominant in the case of two flutes microendmill. From the above, it is observed that, the microendmilling with two flutes is mostly affected by ploughing than that of shearing.

From Fig. 11, it is observed that increasing and decreasing trends of feed force from upmilling (B to C) and downmilling (C to D) in both microendmills as shown in Fig. 4. However, the magnitude of feed force during upmilling is lesser in the case of four flutes microendmill than that of two flutes microendmill.

Figure 12a, b shows the cutting forces behaviour with respect to the uncut chip thickness ( $t$ ) and tool geometry. Feed force is found to be the maximum when the uncut chip thickness ( $t$ ) reaches the maximum limit. From Fig. 12, it is also observed that transverse force approaches nearly zero, when the uncut chip thickness ( $t$ ) is

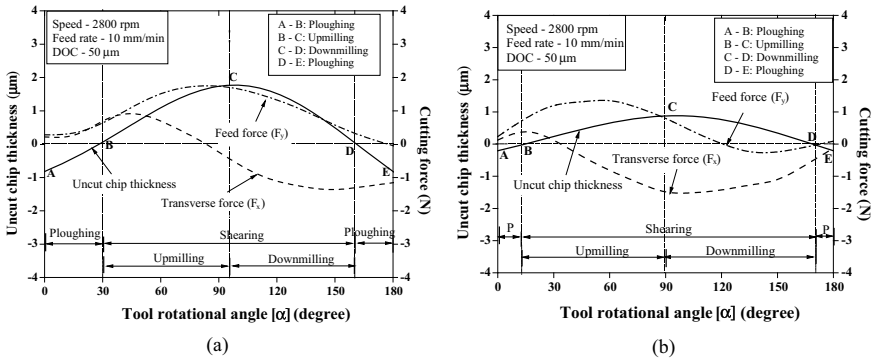


**Fig. 12** Typical behaviour of cutting forces with the uncut chip thickness of different tool geometry in microendmilling. **a** Two flutes microendmill. **b** Four flutes microendmill

found to be the maximum level. The transverse force is found to change the direction from positive direction to negative direction during downmilling (regions C to D) while using two flutes and four flutes microendmill (Fig. 12a, b). By comparing Fig. 12a, b, it is observed that, shearing mode of material removal mechanism is dominant with four flutes than the two flutes microendmill. This may be due to the increase in contact area between the tool and workpiece. Figure 12 also indicates that the transverse force and feed force are found to be lesser in the case of four flutes microendmill due to the reduced uncut chip thickness ( $t$ ).

Figure 13 shows the tool geometry effect on the resultant forces ( $F_r$ ) with various rotational speed and feed rate with the constant depth of cut (50 µm). It is observed that, the rotational speed and feed rate are compounded irrespective of the tool geometry at the lowest speed of 700 rpm, as similar to the conventional endmilling. The same trend is observed by Lai et al. [9]. In conventional endmilling, increased rotational speed and feed rate resulted in the increasing trend of the cutting force

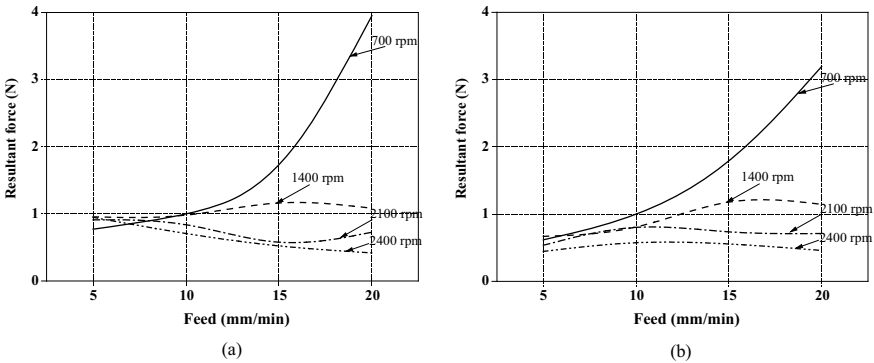


**Fig. 13** Tool geometry effect on cutting forces in microendmilling. **a** Two flutes microendmill. **b** Four flutes microendmill

values [11]. At lower speed of 700 rpm along with increased feed rate, higher cutting forces are observed due to the dominance of rubbing and ploughing. However, when the rotational speed increases above 2100 rpm the resultant forces tends to decrease. In the case of two flutes microendmill, the cutting forces are found to be higher than that of four flutes microendmill due to the effect of ploughing than that of the shearing [28].

## 4 Conclusions

This work presented the investigations on the effect of tool geometries of microendmill with two flutes and four flutes during microendmilling of copper alloy (BSS 249) on the surface roughness ( $R_a$ ), the uncut chip thickness ( $t$ ) and cutting forces (feed and transverse forces). The following conclusions are drawn from the present investigations.

- Four flutes microendmill resulted in lesser  $R_a$  than that of the two flutes microendmill, due to the closer tool path generation of the flutes in the microendmill in the feed direction and also due to the formation of continuous chip. Therefore, to achieve the better  $R_a$  during microendmilling, four flutes microendmill with higher speed and with moderate feed rate is recommended.
- Based on the behaviour of uncut chip thickness ( $t$ ), it is found that both ploughing and shearing are observed during the half tool rotation of the microendmill, irrespective of the rotational speed and feed rate, in both two flutes and four flutes microendmills. However, the size of uncut chip thickness ( $t$ ) and the ploughing effect is found to be lesser while using four flutes. Shearing is found to be dominant during microendmilling with four flutes microendmill due to the increase in contact area of tool–workpiece interface.
- From the cutting forces analyses, it is found that the signature of the cutting force signals for both two flutes and four flutes microendmill are similar with respect to the tool rotational angle. However, significant angular shift is observed in the case of four flutes microendmill due to the closer trochoidal tool path generation of successive passing of microendmill. Transverse and feed forces are found to be low in the case of four flutes microendmill due to the reduced uncut chip thickness ( $t$ ) in the same parametric level of microendmilling. Cutting forces are found to be higher with two flutes microendmill due to the dominance of ploughing than that of the shearing.

## References

1. Masuzawa T (2000) State of the art of micromachining. *Ann CIRP* 49:473–488
2. Alting L, Kimura F, Hansen HN, Bissacco G (2003) Micro engineering. *CIRP Ann Manuf Technol* 52:635–657
3. Dornfeld D, Min S, Takeuchi Y (2006) Recent advances in mechanical micro machining. *CIRP Ann Manuf Technol* 55:745–768
4. Chae J, Park S, Freiheit T (2006) Investigation of micro cutting. *Int J Mach Tools Manuf* 46:313–332
5. Newby G, Venkatachalam S, Liang SY (2007) Empirical analysis of cutting force constants in micro-end-milling operations. *J Mater Process Technol* 41–47:192–193
6. Fang FZ, Wu H, Liu XD, Liu YC, Ng ST (2003) Tool geometry study in micromachining. *J Micromech Microeng* 13:726–731
7. Filiz S, Conley CM, Wasserman MB, Ozdoganlar OB (2007) An experimental investigation of micro-machinability of copper 101 using tungsten carbide micro-endmills. *Int J Mach Tools Manuf* 47:1088–1100
8. Li H, Lai X, Li C, Feng J, Ni J (2008) Modelling and experimental analysis of the effects of tool wear, minimum chip thickness and micro tool geometry on the surface roughness in micro-end-milling. *J Micromech Microeng* 18. <https://doi.org/10.1088/0960-1317/18/2/025006>
9. Lai X, Li H, Li C, Lin Z, Ni J (2008) Modelling and analysis of micro scale milling considering size effect, micro cutter edge radius and minimum chip thickness. *Int J Mach Tools Manuf* 48:1–14
10. Bissacco G, Hansen HN, De Chiffre L (2005) Micromilling of hardened tool steel for mould making applications. *J Mater Process Technol* 167:201–207
11. Koshy P, Dewes RC, Aspinwall DK (2002) High speed end milling of hardened AISI D2 tool steel (~ 58 HRC). *J Mater Process Technol* 127:266–273
12. Matsumura T, Hiramatsu T, Shirakashi T (2005) A study on cutting force in the milling process of glass. *J Manuf Process* 7(2):102–108
13. Li HZ, Zhang WB, Li XP (2001) Modelling of cutting forces in helical endmilling using predictive machining theory. *Int J Mech Sci* 43:1711–1730
14. Tansel I, Rodriguez O, Trujillo M, Paz E, Li W (1998) Micro-end-milling: I. Wear and breakage. *Int J Mach Tools Manuf* 38:1419
15. Friedrich CR, Coane PJ, Vasile MJ (1997) Micromilling development and applications for micro-fabrication. *J Microelectron Eng* 35:367
16. Bao WY, Tansel IN (2000) Modeling micro-end-milling operations. Part II: tool run-out. *Int J Mach Tools Manuf* 40:2175–2192
17. Fang FZ (2002) Cutting edge effect in micromachining. Presentation to the Cutting Committee Meeting (Part II) in 52nd CIRP General Assembly (Spain)
18. Mian AJ, Driver N, Mativenga PT (2011) Identification of factor that dominate the size effect in micro-machining. *Int J Mach Tools Manuf* 51:383–394
19. Yun HT, Heo S, Lee MK, Min BK, Lee SJ (2011) Ploughing detection in micromilling process using the cutting force signal. *Int J Mach Tools Manuf* 51:377–382
20. Srinivasa YV, Shunmugam MS (2013) Mechanistic model for prediction of cutting forces in microendmilling and experimental comparison. *Int J Mach Tools Manuf* 67:18–27
21. Sooraj VS, Mathew J (2011) An experimental investigation on the machining characteristics of microscale endmilling. *Int J Adv Manufa Technol* 56:951–958
22. Kang IS, Kim JS, Seo YW (2010) Investigation of cutting force behaviour considering the effect of cutting edge radius in the micro-scale milling of AISI 1045 steel. *Proc IMechE* 225:163–171
23. Malekian M, Park SS, Jun MBG (2009) Modeling of dynamic micro-milling cutting forces. *Int J Mach Tools Manuf* 49:586–598
24. Park SS, Malekian M (2009) Mechanistic modeling and accurate measurement of microend-milling forces. *CIRP Ann Manuf Technol* 58:49–52

25. Cuba Ramos A, Autenrieth H, Straub T, Deuchert M, Hoffmeister J, Schulze V (2012) Characterization of transition from ploughing to cutting in micromachining and evaluation of minimum chip thickness of cut. *J Mater Process Technol* 212:594–600
26. Afazov SM, Zdebski D, Ratchev SM, Segal J, Liu S (2013) Effect of micro-milling conditions on the cutting forces and process stability. *J Mater Process Technol* 213:671–684
27. Prakash M, Kanthababu M (2013) In-process tool condition monitoring using acoustic emission sensor in microendmilling. *Int J Mach Sci Technol* 17(2):209–227
28. Chen W, Teng X, Huo D, Wang Q (2017) An improved cutting force model for micro milling considering machining dynamics. *Int J Adv Manuf Technol* 93(9–12):3005–3016
29. Sahoo P, Patra K (2019) Mechanistic modeling of cutting forces in micro-end-milling considering tool run out, minimum chip thickness and tooth overlapping effects. *Mach Sci Technol* 4;23(3):407–430
30. Chen W, Huo D, Teng X, Sun Y (2017) Surface generation modelling for micro end milling considering the minimum chip thickness and tool runout. *Proc CIRP* 1(58):364–369